12 Magnetic and Thermal Properties of Superconducting and Related Materials

H. Keller, C. Aegerter (till Jan. 99), J. Hofer, V.A. Ivanshin (visiting scientist), B.I. Kochelaev (visiting scientist), A. Schilling, A. Shengelaya, M. Willemin, G.M. Zhao, and K.A. Müller (Honorarprofessor)

12.1 Introduction

Over the past year we have continued and extended our investigations of the magnetic properties of high-temperature superconductors (HTS) and related magnetic systems. In order to achieve this goal we have used a combination of muon spin rotation (μSR), neutron scattering, electron paramagnetic resonance (EPR), together with bulk SQUID and torque magnetometry, and thermal measurements.

During the last year we have continued our muon-spin rotation (μSR) and neutron scattering experiments on the structure of the magnetic field distributions in superconductors (see Sec. 12.2). Apart from the well established neutron scattering investigations at the Institut Laue-Langevin (ILL), we have this year also had the opportunity to carry out experiments on the new spallation source SINQ at the Paul Scherrer Institut (PSI). These investigations at PSI will hopefully in the future complement the work at ILL. Moreover, we have extended our detailed investigations of the magnetic penetration depth in cuprate and related superconductors to the $YBa_2Cu_4O_8$ family (see Sec. 12.3).

In the last year we have further developed the technique to study vortex matter in highly anisotropic superconductors by means of ultrasensitive torque magnetometry (see Sec 12.4). In particular, we have demonstrated that the application of an additional oscillating magnetic field perpendicular to the main field may affect dramatically the irreversibility of high-temperature superconductors. The reversible domain in the (H, T) phase diagram can be extended, which is of particular interest for torque investigations in samples dominated by pinning. Ultrasensitive torque magnetometry measurements on untwinned single crystal of $YBa_2Cu_3O_{7-\delta}$ reveal that the vortex-lattice melting transition is unaffected by this additional ripple magnetic field.

In a further project, we have completed a detailed thermal and magnetic study on the angular dependencies of the discontinuities in entropy and in magnetization at the first-order vortex-lattice melting transition in untwinned $YBa_2Cu_3O_{7-\delta}$. We have also built up a new sensitive heat capacity device (estimated resolution 10^{-10} J/K) that can be operated between 40 K and 300 K, and in magnetic fields up to 10 T (see Sec 12.5).

We have continued our studies of oxygen-isotope effects in the magnetoresistive manganites $Ln_{1-x}A_xMnO_3$ (Ln is a rare-earth element, A is a divalent element) using magnetization and resistivity measurements (see Sec. 12.6.1). We found that the exponent of the oxygen-isotope effect on the Curie temperature T_C is simply proportional to the pressure-effect coefficient, and is a unique and simple function of T_C in the composition region where there is a metallic ground state. The results clearly show that the giant oxygen-isotope effects observed in the manganites are intrinsic, which give strong evidence for the polaronic nature of charge carriers in these materials. We have also studied the oxygen-isotope effect on the charge-ordering transition in $Nd_{0.5}Sr_{0.5}MnO_3$ and $La_{0.5}Ca_{0.5}MnO_3$. As the main result of this study, we discovered a colossal oxygen-isotope shift (> 40 K) of the charge-ordering transition temperature in both materials when a magnetic field of 5.4 T is applied. The isotope effect increases rapidly with increasing magnetic field. These results clearly establish that the strong electron-phonon coupling plays an essential role in the charge-ordering of manganites. Furthermore, we have studied the oxygen-isotope effects on the stripe formation temperature T^*, and on the local structure deviations in the single-layer cuprate superconductors $La_{2-x}Sr_xCuO_4$., using x-ray absorption near-edge spectroscopy (XANES) (see Sec. 12.6.2). We found a very large oxygen isotope shift of T^*. Upon replacing ^{16}O with ^{18}O, the stripe formation temperature in $La_{1.94}Sr_{0.06}CuO_4$ increases from about 110 K to 170 K. Furthermore, the amplitude of the dynamic lattice distortions strongly depends on the oxygen isotope mass, that is, the amplitude of the distortion in the ^{18}O sample is much larger than that in the ^{16}O sample. These results will place important constraints on the microscopic origin of the stripe phase and on the microscopic mechanism of high-temperature superconductivity.

Electron Paramagnetic Resonance (EPR) is a powerful tool in solid state physics, which allows to study crystal electric fields, electron-phonon interactions, static and dynamic magnetic correlations on a *microscopic* level. EPR is a contact-less method, thus samples of any form (powder, pellet, single crystal, thin film) can be measured. Due to the extreme sensitivity of EPR, only a tiny amount of material is necessary. Our research interest during the last year was mainly concerned with oxygen isotope effects in high-T_c cuprates (see Sec. 12.6.3).

This work was done in collaboration with scientists from ETH Zürich (G. Blatter, K. Conder, J. Karpinski, and G.I. Meijer), IBM Rüschlikon Research Laboratory (C. Rossel), University of Birmingham (E.M. Forgan, S.H. Lloyd, T. M. Riseman, T. J. Jackson, and P.G. Kealey), University of St. Andrews (S.L. Lee, F. Y. Ogrin, and C. Ager), Institut Max von Laue-Paul Langevin, Grenoble (R. Cubitt), University of Oxford (S.J. Blundell and B. W Lovett), RIKEN-RAL (F.L. Pratt), University of Warwick (D. McK. Paul and N. Bancroft), Oak Ridge National Laboratory (M. Yethiraj), Tohoku University (T. Sasaki), and Université Paris-Sud (S.T. Johnson and A. Revcolevschi), University of Maryland (R. L. Greene and K. Ghosh), University of Rome (A. Bianconi, N. L. Saini, and A. Lanzara), University of Berkeley (R.A. Fisher and N.E. Phillips), Los Alamos National Laboratory (M. Hundley and A. Lacerda), Argonne National Laboratory (U. Welp, W.K. Kwok, R.J. Olsson, and G.W. Crabtree), Institute of Low Temperature and Structure Research, Polish Academy of Sciences, Wroclaw, Poland (P.W. Klamut), Northern Illinois University, DeKalb, USA (B. Dabrowski), and Kazan State University, Russia(B.I.Kochelaev).

12.2 Investigating vortex matter at central facilities

The microscopic methods of muon spin rotation (μSR) and neutron small angle scattering (SANS) are ideal tools to investigate many facets of condensed matter systems. In our work we have been primarily occupied with investigating the structure and dynamics of magnetic flux-lines in superconductors. These structures are interesting in themselves, as they present a type of 'matter' whose microscopic structure (magnetic field) and interactions are well understood, but whose mesoscopic behavior is far from trivial. On a more applied note, the understanding of flux-lines sheds light on the superconducting properties of a specific system (as e.g. the low-temperature superconductor Sr_2RuO_4) and thus the superconducting mechanism of the material in question.

During the last years we have also started the investigation of the superconducting behavior of Sr_2RuO_4 (SRO). SRO is a superconductor, which is isostructural to the high-T_c cuprates, but does not contain copper [1]. Beside this obvious similarity, there are however also many differences that make SRO a research subject in its own right. Its electronic behavior differs in many respects and in the normal state can be well described by an anisotropic Fermi liquid [2]. This, together with the strong Hund's rule coupling and the ferromagnetic nature of the relative compound $SrRuO_3$, has lead to the theoretical expectation of very unusual superconducting behavior [3, 4]. It is thought that similar to superfluid He-3, the pairing (of electrons) in SRO is in a triplet state, making SRO a p-wave superconductor. This makes it an exciting field of research decoupled from the HTS. The supposed p-wave nature of the superconductivity in SRO may also lead to very unconventional behavior of the flux line lattice in this material [4]. In the course of our studies using both SANS [5] and μSR [6], we have found that the vortex lattice is of a square symmetry. In μSR, this has been inferred from the detailed shape of the internal field distribution, determined by the positions of the minimum, maximum and saddle point fields as shown in Fig. 12.1. The SANS pattern, shown in the insert of Fig. 12.1, was taken subsequently to the μSR experiments and confirms the earlier findings. The samples used in the investigations were from different sources with different levels of impurities, indicating that the squareness of the lattice is independent of the amount of impurities. This may arise from several reasons, such as a combination of non-local interactions and in-plane anisotropy. These effects have for instance been shown to give rise to unconventional (in some cases square) flux-lattices in superconductors of the Nickelborocarbide family [7]. In SRO a square lattice may also arise from the predicted effects of a p-wave symmetry of the supercarriers [4].

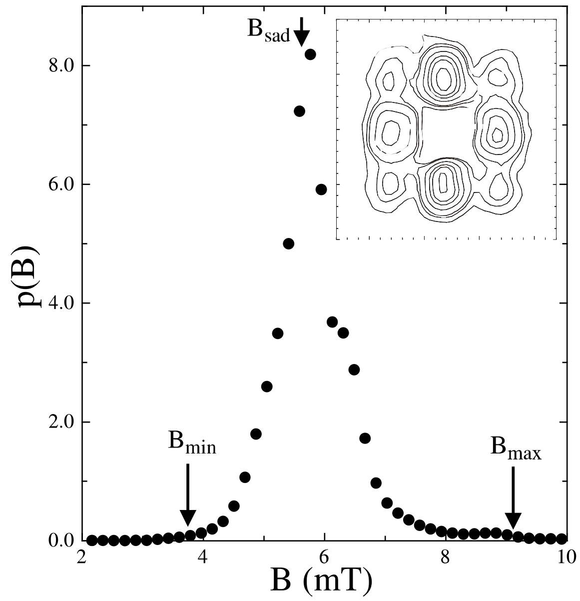

Figure 12.1: *The μSR lineshape $p(B)$ in SRO taken after cooling from above T_c in an applied field of 6mT. From the relative positions of the characteristic fields B_{min}, B_{max} and B_{sad}, we may induce the symmetry of the vortex lattice [6]. The insert shows a neutron diffraction pattern at a field of 20 mT.*

Measurements of the temperature dependence of the penetration depth that is observable via the second moment of the field distribution and the scattered neutron intensity would be able to give further confirmation of the pairing state. In simple constant node theories of p-wave superconductivity [3] a saturation at low temperatures is expected. Our current measurements on this subject are still ambiguous and probably influenced by impurities. In order to further investigate the occurrence of a square flux-line lattice in this material, we also currently perform additional measurements with the applied field away from the high symmetry c-axis, which will allow us to discard possibilities like anisotropy or non-local effects due to the high anisotropy of the material. With the field at an angle, the upper critical field is increased considerably, leading to a strong reduction in non-local interactions. Furthermore, a possible in-plane anisotropy also becomes negligible due to the high c-axis anisotropy.

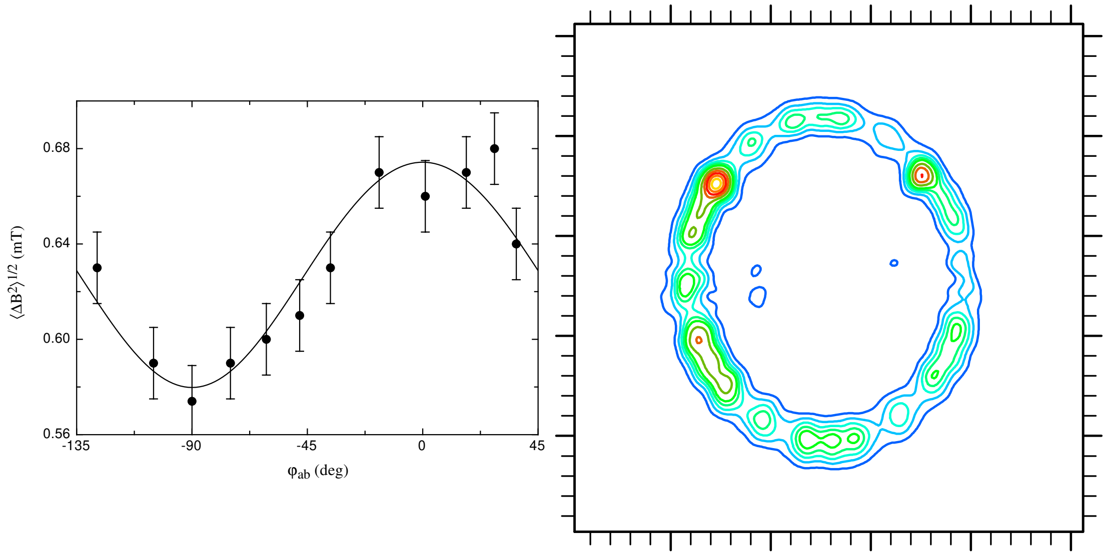

Figure 12.2: *The angular dependence of the second moment of the internal field distribution (left) and the neutron diffraction pattern for an untwinned sample (right). This gives a measure of the ab-anisotropy in the penetration depth.*

Due to the supposed d-wave pairing symmetry one might also expect unconventional vortex structures in the high-temperature superconductors (HTS). In many of these systems however, there are additional complications, such as the dimensional break-up of the vortex-lattice at fields much lower than H_{c_2} in $Bi_2Sr_2CaCu_2O_{8+\delta}$ or twin-plane boundaries acting as strong pinning sites [8] in $YBa_2Cu_3O_{7-x}$ (YBCO) and anisotropic superconducting behavior in the crystallographic ab-planes. How these properties influence the structure of the vortex lattice in YBCO has been studied. We find that in heavily twinned samples, the effect of the pinning to twin boundaries dominates the observed structure leading to a fourfold diffraction pattern in SANS. This symmetry arises from the presence of both orientations of the ab-planes and does not correspond to a square lattice as has been claimed [9]. Even in nominally untwinned samples, there are still remaining influences of the pinning to twin boundaries. However, the ab-anisotropy in an untwinned sample is clearly observable in both neutron scattering and μSR. In the case of μSR the in-plane anisotropy is determined from the change in the width of the internal field distribution as the field is applied at different angles to the a-axis within the plane. The anisotropy also gives rise to the ellipsoidal shape of the scattering pattern in SANS, thus allowing a measurement of the anisotropy-parameter. This is illustrated in Fig. 12.2. Both methods determine the ab-anisotropy to be $\gamma_{ab} = 1.16(2)$ [10].

In addition, we have studied the melting of the vortex lattice in twinned and untwinned samples, where the melting is at much higher temperatures than for instance in BSCCO [11]. We find good agreement with specific heat [12, 13] and torque measurements [14] on similar crystals. The observed transition in twinned samples is gradual, consistent with being of second order. In the untwinned samples however, the transition is sharper down to low fields. Given the size of the crystals used in the investigation this is not inconsistent with a first order transition [13]. Furthermore, the melting temperatures are only weakly influenced by the presence of the twin planes, again in accord with specific heat measurements [12], and are in fair agreement with anisotropic scaling theory and latent heat measurements [15].

12.3 Penetration depth measurements in $YBa_2Cu_4O_8$ family superconductors

The magnetic field penetration depth λ is one of the fundamental lengths of a superconductor. The temperature dependence $\lambda(T)$ reflects the quasiparticle density of states available for thermal excitations and therefore probes the superconducting gap structure. A systematic and comprehensive study of the penetration depth and its temperature dependence in various families of cuprates is important for understanding the occurrence of superconductivity in these materials.

Detailed μSR investigations of polycrystalline high-temperature superconductors (HTS) have demonstrated that λ can be obtained from the μSR depolarization rate $\sigma(T) \sim 1/\lambda^2(T)$ [16]. Early μSR studies on polycrystalline HTS have concluded that σ has a weak temperature dependence for $T \ll T_c$, suggesting there is an energy gap in the spectrum of excitations, as expected for conventional s-wave pairing. On the other hand, more recent μSR measurements on high-quality $YBa_2Cu_3O_{7-\delta}$ (Y123) single crystals revealed a linear temperature dependence of σ up to $0.4T_c$ [17]. It is not clear why μSR measurements in polycrystalline and single crystal samples give different $\lambda(T)$ dependencies at low temperatures. It was suggested that small amounts of impurities or other crystalline imperfections can change the low-temperature behavior $\lambda(T)$ from a linear to a quadratic dependence [17], which is difficult to distinguish from the conventional BCS behavior without precise low- temperature data.

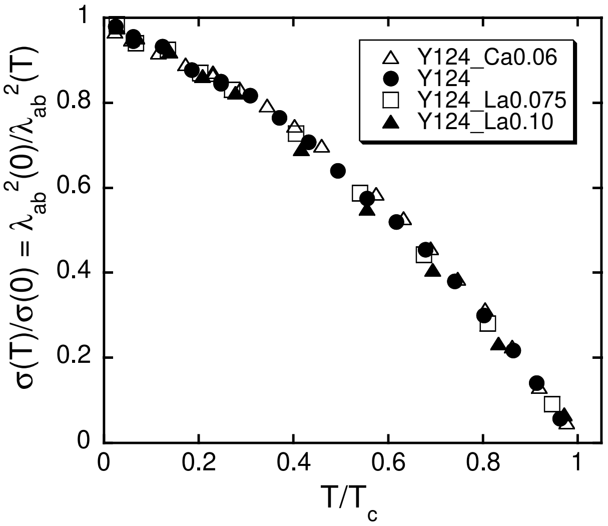

Figure 12.3: *Normalized depolarization rate $\sigma(T)/\sigma(0)$ as a function of reduced temperature T/T_c for pure, Ca- and La- doped Y124 superconductors.*

We have decided to study this problem in some detail by investigating the penetration depth in $YBa_2Cu_4O_8$ (Y124) with a special attention to the low-temperature behavior. The structure of Y124 is distinguished by its high thermal stability and fixed oxygen stoichiometry with well-ordered double CuO chains. We have investigated polycrystalline Ca- and La-doped $YBa_2Cu_4O_8$ superconductors with T_c ranging from 72 to 88 K [18]. It was found that in all samples $\sigma(T)$ is a linear function of T below ~25 K. In Fig. 12.3 we plot the normalized depolarization rate $\sigma(T)/\sigma(0)$ versus the reduced temperature $t = T/T_c$ so that the temperature dependencies for samples with different doping levels can be compared directly. It is seen that all samples exhibit quite a similar temperature dependence. Such a scaling behavior has recently been found by Hardy *et al.* [19] for single-crystal $YBa_2Cu_3O_{7-\delta}$

with δ=0.01, 0.05, and 0.40 from surface impedance measurements. This observation puts important constraints on models proposed to explain the linear temperature dependence of the penetration depth in HTS at low temperatures.

12.4 Investigating vortex matter by torque magnetometry

12.4.1 Enhancement of the vortex-lattice relaxation by means of an external ac magnetic field

Torque magnetometry has proven to be a useful method for determining superconducting parameters such as the in-plane penetration depth λ_{ab}, the in-plane coherence length ξ_{ab}, and especially the effective mass anisotropy γ in HTS. These parameters are generally derived by fitting the measured angular-dependent reversible torque with a theoretical expression derived by Kogan and coworkers [20] for a three-dimensional (3D) anisotropic superconductor in the mixed state. However, for a reliable analysis, the reversibility of the torque curves is required, i.e., the vortex lattice must be in a reversible state, corresponding to its thermodynamical equilibrium. Unfortunately, in most superconductors, only a narrow reversible range in the field-temperature (H, T) phase diagram below the upper critical field $H_{c2}(T)$ can be explored, owing to the onset of irreversibility by pinning effects at lower T. Moreover, close to T_c, the distorsion of the torque signal due to the domination of thermal fluctuations has been predicted theoretically and observed experimentally [21]. In this regime, it is almost impossible to get a reliable value of γ. On the other hand, in a not too strong pinning regime, it is possible to analyze the reversible curve approximated by $\tau_{rev}(\theta) \simeq \frac{1}{2}(\tau^{+}(\theta) + \tau^{-}(\theta))$. However, in the presence of a large irreversiblity, the anisotropy γ extracted in this way is overestimated.

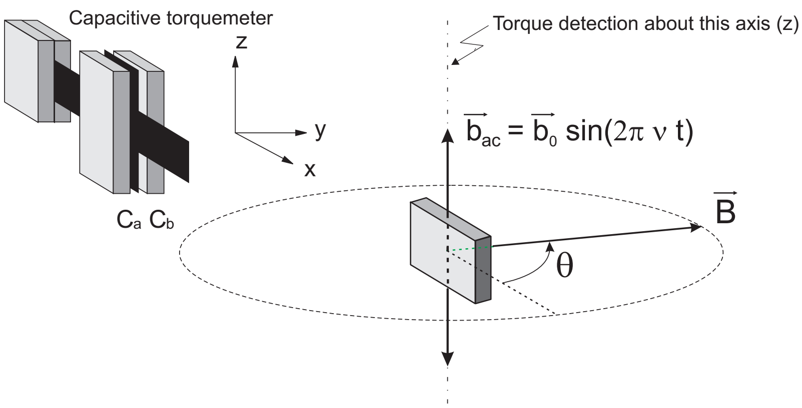

Figure 12.4: *Geometrical configuration for the "vortex-shaking procedure" during an angular-dependent torque measurement. $\vec{B}$ and $\vec{b}_{ac}$ denote the main and the weak ac field, respectively.*

In order to extend the reversible regime, a new method has been developed [22]. The application of a transverse ac magnetic field to the main magnetic field "shakes" the vortices out of their pinning potential, which enhances the relaxation of the flux-line lattice (FLL) towards its thermodynamical equilibrium (see Fig. 12.4). The vortex-shaking method is compatible with capacitive [23] as well as piezoresistive torque sensors [24] (see also Annual Reports 96/97 and 97/98). The power of this technique has been verified in several HTS compounds. A typical set of angular-dependent torque measurements for an untwinned single crystal of $YBa_2Cu_3O_{7-\delta}$ with and without FLL shaking is displayed in Fig. 12.5. In the absence of an oscillating field (no FLL shaking) the reversible torque curve $\tau_{rev}(\theta)$ can by fitted

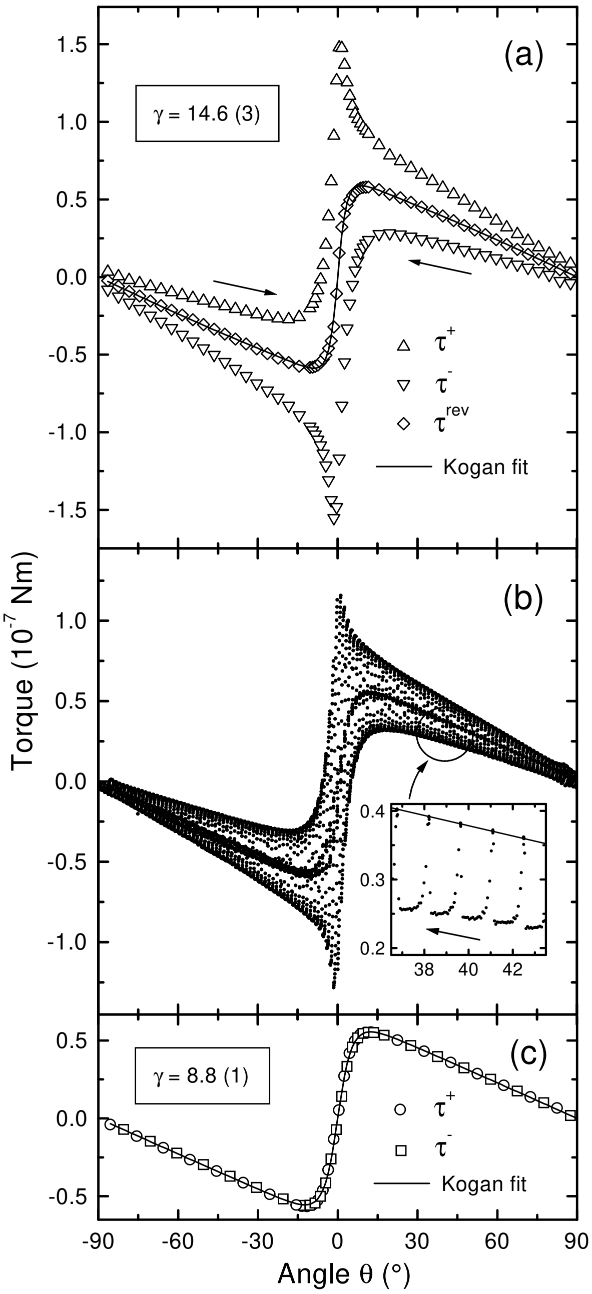

Figure 12.5: *Angular-dependent torque measurements in the ac plane on an untwinned single crystal of $YBa_2Cu_3O_{7-\delta}$ ($\theta = 0°$ for $\vec{B}$ parallel to the ab-plane). (a) Torque for clockwise (τ^+) and counterclockwise (τ^-) rotations of $\vec{B}$ obtained without FLL shaking at $T = 91.2$ K, $B = 0.1$ T and $d\theta/dt = 110°/min$. The solid line represents the fit to $\tau_{\rm rev}(\theta) \simeq 1/2(\tau^+(\theta)+\tau^-(\theta))$ with Kogan's expression, yielding $\gamma \simeq 14.6(3)$. (b) Similar measurements as in (a), but with vortex shaking. Details of relaxation sequences are shown in the inset. (c) The fit after FLL shaking gives $\gamma = 8.8(1)$. The curves are fully reversible in this case.*

by the expression given by Kogan *et al.* [20] (Fig. 12.5(a)). By doing so, an unrealistically high value γ =14.6(3) is obtained, which is explained by the large irreversibility that peaks at $\theta \simeq 0$, i.e., for $\vec{B}$ close to the ab plane of the sample. The above expression for $\tau_{rev}(\theta)$ is not suitable in this case. However, by applying the shaking procedure to the crystal at the same field ($B = 0.1$ T) and temperature ($T = 91.2$ K), a fully reversible curve is obtained as shown in Fig. 12.5(b). By considering only the data after the FLL relaxation, the fit leads to a realistic anisotropy $\gamma = 8.8(1)$ (Fig. 12.5(c)). For investigations of HTS in the mixed state this method is not only restricted to torque magnetometry, but can also be used by other techniques, like specific heat or resistivity.

12.4.2 First-order vortex-lattice melting transition in $YBa_2Cu_3O_{7-\delta}$ near the critical temperature detected by magnetic torque

Recent experimental work on the vortex-lattice melting in HTS clearly showed that the melting transition from the ordered vortex solid to a vortex-fluid phase, at the so-called "melting temperature" T_m, is of first order [25]. A first-order transition is characterized by a discontinuity ΔS in the entropy $S = -(\partial F/\partial T)_{\mathrm{H}}$. This entropy discontinuity ΔS can be related to a discontinuity in the magnetization ΔM, according to the Clausius-Clapeyron equation

$$\Delta S = -\Delta M \mu_0 \frac{dH_m^c}{dT}. \tag{12.1}$$

Note that the melting temperature T_m depends on the applied magnetic field $\mu_0 H$, which forms the "melting line" $H_m(T)$ in the (H, T) phase diagram. Torque magnetometry is a very powerful tool for detecting the vortex-lattice melting transition (VLMT). Indeed, the discontinuity in magnetization ΔM is related to a step in the torque signal $\Delta\tau$. In a first approximation, assuming a magnetization perpendicular to the Cu-O planes of the crystal, the step in the torque signal is given by $\Delta\tau = V \Delta M \mu_0 H \cos\theta$, where V is the volume of the sample, and θ is the angle between the applied magnetic field $\vec{H}$ and the Cu-O planes.

Figure 12.6(a) shows the VLMT as observed by field-dependent torque measurements taken at $T = 90.70$ K ($T_c = 93.3$ K) and different field-sweep rates. The solid phase is characterized by an irreversible behavior of the torque, which disappears in the fluid phase. At low sweep rates, the torque signal shows clearly more intrinsic noise. This is due to the fact that vortices discontinuously enter or leave the sample in successive flux bundles, while the magnetic field is swept. By adding a weak ac transverse magnetic field (vortex shaking), the irreversibility in the solid phase can be shifted down to lower magnetic fields (Fig. 12.6(b)). This offers the possibility to tune the irreversibility, leaving the VLMT unchanged. We performed a systematic study of the VLMT in $YBa_2Cu_3O_{7-\delta}$ by ultrasensitive torque magnetometry, especially near the critical temperature T_c (Ref. [14]). The novel results obtained in this study complement previous results from specific-heat measurements [26].

12.5 Detection of small thermal effects in basic and applied condensed matter physics

We have completed a detailed thermal and magnetic study on the angular dependencies of the discontinuities in entropy and in magnetization at the first-order vortex-lattice melting transition in untwinned $YBa_2Cu_3O_{7-\delta}$.

The melting lines $H_m(T, \vartheta)$, (where ϑ is the angle between the applied magnetic field $\vec{H}$ and the c-axis of the crystal), as defined by the thermal experiments, scale perfectly according to recent scaling rules for anisotropic superconductors, with an anisotropy parameter $\gamma \approx 8$.

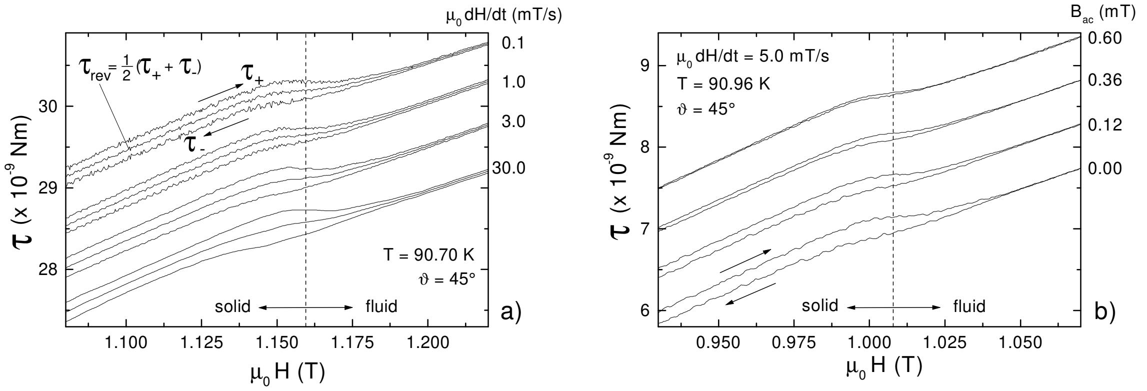

Figure 12.6: *The phase transition associated with vortex-lattice melting (dashed vertical line) as observed by field-dependent torque measurements on an untwinned single crystal of YBCO. (a) Magnetic torque τ for increasing (τ_+) and decreasing (τ_-) magnetic field $\mu_0 H$ for different sweep rates $\mu_0 dH/dt$, taken at 90.70 K and $\vartheta = 45°$. The data reveal a constant magnetization jump ΔM at the VLMT, determined from the reversible torque curve τ_{rev}. (b) Similar measurements (90.96 K, $\vartheta = 45°$) with an additional weak transverse ac magnetic field B_{ac} show a progressive suppression of irreversibility, remaining the VLMT itself unaffected. In both figures each set of data is vertically shifted for clarity.*

In the temperature range 81 K $< T < T_c =$ 92 K and for any choice of ϑ, the discontinuity in entropy at melting, ΔS per unit volume of sample, depends solely on the temperature T where melting occurs, but does not depend on ϑ and the corresponding applied magnetic field $H_m(T, \vartheta)$, which is in full agreement with these scaling rules [26]. The temperature dependence of $\Delta S(T)$ near the critical temperature T_c, can be quantitatively explained by a recently developed theory that accounts for the strong T dependence of the model parameters near T_c for the London model describing the thermodynamics of the vortex system [27]. Along with the discontinuities in entropy due to the latent heat, nearly step-like increases in the specific heat of $YBa_2Cu_3O_{7-\delta}$ at the vortex-lattice melting temperature are observed [26]. These increases are reflected in changes in the slope $\Delta(\partial S/\partial T)_{\mathrm{H}}$ at the melting temperature. However, the thermal data alone do not allow to conclude whether or not these slope changes depend only on T as predicted by theory.

To clarify these issues we performed a series of magnetization measurements on a different crystal in our home built torque magnetometer, in the temperature range 91 K $< T < T_c =$ 93.3 K (in collaboration with C. Rossel, IBM Rüschlikon Research Laboratory). We measured the torque $\vec{\tau} = V\vec{M} \times \mu_0 \vec{H}$ at a fixed temperature T for different magnetic fields H, and varied the angle ϑ. The resulting discontinuities at the melting transition are $\Delta\tau(\vartheta)$, with associated changes in slope $\Delta(\partial\tau/\partial H)_{\mathrm{T}}$. In this way, the transverse component of the discontinuity $\Delta\vec{M}$ in magnetization $\vec{M}$ can be directly measured. However, the smallness of both the investigated crystal and the effect to be observed, does not allow for a direct measurement of the longitudinal component of $\Delta\vec{M}$, e.g., using a SQUID magnetometer. We derive this component indirectly from thermodynamics. We use the fact that ΔS depends only on T, and the Clausius-Clapeyron formula gives an additional restriction. In this way we were able to determine both components of the vector $\Delta\vec{M}$, and to study its rotation when the angle ϑ approaches the direction of the Cu-O planes.

The final result is that the vector $\Delta\vec{M}$ is always directed parallel to the total magnetization $\vec{M}$ (but not necessarily parallel to the c-axis), and is rotating away from c by the angle φ

according to $\tan\varphi = \tan\vartheta/\gamma^2$. The corresponding changes in slope, $\Delta(\partial\tau/\partial H)_{\mathrm{T}}$, strongly depend on ϑ. They can be translated to discontinuities in specific heat using rather complex thermodynamic relations, and turn out to be independent of ϑ as expected by theory. The agreement between all these magnetic data and the thermal data is excellent. The anisotropy parameter γ can be extracted form all these measurements, and turns out to be constant ($\gamma \approx 8.2$) up to the highest investigated temperature ($T = 92.4$ K).

We have also done an additional series of thermal measurements in magnetic fields up to 18 T, to study the critical endpoint of the vortex-lattice melting line, and to investigate whether or not there are additional phase boundaries in the magnetic phase diagram (in collaboration with the Los Alamos National Laboratory, Los Alamos, USA). The critical point in the investigated sample is at $\mu_0 H = 12$ T for $\vec{H} \parallel c$. Measurements at fixed temperature and in varying magnetic field allowed us to investigate the thermomagnetic behavior both below and above the vortex-lattice melting line. There is no conclusive thermal sign of a horizontal phase boundary as suggested by theory, that should indicate the transition (or crossover) from a 3D-like to a 2D-like vortex dynamics.

We have built up a new sensitive heat capacity device that is based on a differential calorimetry technique [28]. It can be operated between 40 K and 300 K, and in magnetic fields up to 10 T. The sample holder can be rotated in the magnetic field, and allows therefore for convenient angular dependent heat-capacity experiments. With a new design and improved thermometry, we are able to achieve a resolution in heat capacity that is improved by a factor of 100 compared to the standard technique [28].

12.6 Studies of oxygen isotope effects

12.6.1 Oxygen isotope effects in the manganites

The giant oxygen-isotope shift of the Curie temperature T_C in $\mathrm{La_{0.8}Ca_{0.2}MnO_{3+y}}$ discovered by us [29] provides crucial evidence for the existence of small polarons (Jahn-Teller (JT) polarons [30]) in these materials, and place important constraints on the microscopic mechanism of the colossal magnetoresistance effect. However, some physicists have raised criticisms on those isotope-effect experiments by speculating that the observed oxygen-isotope effects have nothing to do with a strong electron-phonon interaction, but are caused by the presence of excess oxygen. In order to address this issue, we systematically studied the oxygen-isotope effects in $\mathrm{Ln_{1-x}A_xMnO_3}$ as a function of x and of T_C, and compared the results with the pressure effect data. We found that the exponent of the oxygen-isotope effect on the Curie temperature T_C is simply proportional to the pressure-effect coefficient, and is a unique and simple function of T_C in the composition region where there is a metallic ground state (see in Fig. 12.7). The results clearly show that the observed oxygen-isotope effects in the manganites are intrinsic. There are no correlations between the oxygen-isotope effects and the excess oxygen; the oxygen-isotope exponent is a unique function of T_C.

The real-space ordering of charge carriers in crystals is one of the most interesting phenomena in condensed matter physics. Such a charge-ordering state has been observed mostly in transition-metal based oxides, such as $\mathrm{Ti_4O_7}$ [31], $\mathrm{La_{2-x}Sr_xNiO_4}$ [32], $\mathrm{(La,Pr,Nd)_{0.5}Ca_{0.5}MnO_3}$ [33, 34], $\mathrm{(Pr,Nd)_{0.5}Sr_{0.5}MnO_3}$ [35, 36], etc. In particular, the charge-ordering in manganites is rather exotic. As an example, the charge-ordering state in the manganites $\mathrm{Nd_{0.5}Sr_{0.5}MnO_3}$ and $\mathrm{Pr_{0.5}Sr_{0.5}MnO_3}$ can be destroyed by a small magnetic field (< 10 Tesla) [35, 36]. Theoretically, it has been proposed that the long-range Coulomb repulsive interaction among conduction carriers might be responsible for the charge-ordering in these systems [37, 38, 39].

Our isotope experiments do not support these theoretical models. There is a large oxygen isotope effect on the charge-ordering transition temperature in both $\mathrm{Nd_{0.5}Sr_{0.5}MnO_3}$ and

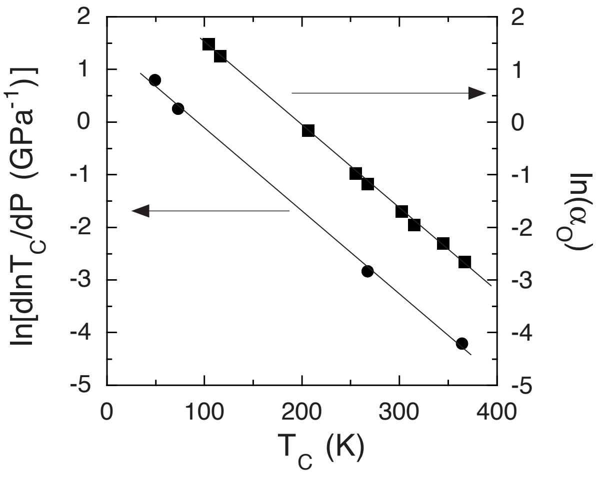

Figure 12.7: *The pressure-effect coefficient β (for a fixed x = 0.3) and the oxygen-isotope exponent α_O (0.2 < x < 0.33) as a function of T_C.*

$La_{0.5}Ca_{0.5}MnO_3$. In Fig. 12.8, we show the temperature dependence of the normalized magnetizations for the ^{16}O and ^{18}O samples of $Nd_{0.5}Sr_{0.5}MnO_3$ under a magnetic field of 2.5 T. The transition from a high magnetization to a low magnetization state is a signature of the transition from a ferromagnetic to a charge-ordering (CO) state. It is clear that there is a large oxygen isotope shift ($\sim$ 20 K) of the charge-ordering transition temperature T_{CO}, and that the shift is completely reversible upon the oxygen isotope back-exchange. Furthermore, we found that with an increase of the external magnetic field, the charge-ordering temperatures of both ^{16}O and ^{18}O samples decrease, but the decreasing rate for the ^{18}O sample is much slower than for the ^{16}O sample. This leads to a dramatic increase in the oxygen isotope shift with increasing magnetic field.

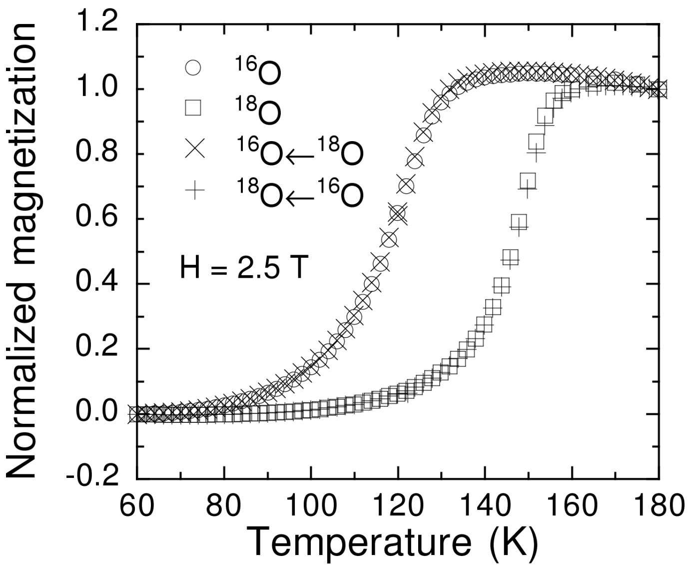

Figure 12.8: *Oxygen-isotope effect on the charge-ordering transition in $Nd_{0.5}Sr_{0.5}MnO_3$ and the oxygen isotope back-exchange result.*

The observed large oxygen-isotope shift of the charge-ordering temperature and its strong dependence on the applied magnetic field are difficult to understand on the basis of the existing theories. In most theoretical models, the charge-ordering arises from a long-range Coulomb repulsive interaction between carriers [37, 38, 39]. So these models predict no isotope effect, and cannot explain our present results.

12.6.2 Oxygen isotope effects in $La_{2-x}Sr_xCuO_4$

One of the outstanding features of cuprate superconductors is the formation of alternative spin and charge stripes below a characteristic temperature [40, 41]. Various x-ray absorption spectroscopic measurements [42, 43, 44] suggest that the local structures in the alternated stripes are different, forming an incommensurate superlattice. Such a stripe phase is believed to be important to the understanding of the pairing mechanism of high-temperature superconductivity. However, the microscopic origin of the stripe phase is still highly debated. It could be caused by purely electronic interactions and/or by a strong electron-phonon coupling. In order to assess whether the latter interaction plays an important role in this phenomenon, we studied the isotope effects on the stripe formation temperature and on the local lattice distortions. We found a very large oxygen isotope shift of the stripe formation temperature in $La_{1.94}Sr_{0.06}CuO_4$ from x-ray absorption spectroscopic study. Upon replacing ^{16}O with ^{18}O, the stripe formation temperature in $La_{1.94}Sr_{0.06}CuO_4$ increases from about 110 K to 170 K. Furthermore, the amplitude of the dynamic lattice distortions strongly depend on the oxygen isotope mass, that is, the amplitude of the distortion in the ^{18}O sample is much larger than that in the ^{16}O sample. Such a huge oxygen-isotope effect cannot be explained by any theoretical models which have ignored a strong electron-phonon interaction. The results will place important constraints on the microscopic origin of the stripe phase and on the microscopic mechanism of high-temperature superconductivity.

12.6.3 EPR study of oxygen isotope effect in $La_{2-x}Sr_xCuO_4$

Cuprate superconductors are known to exhibit a strong Jahn-Teller (JT) effect, which can lead to JT polaron formation. It is well known that the important theoretical concept of JT polarons proposed by Höck et al. [30] led to the original discovery of high-temperature superconductivity [45].

To check this possibility we decided to perform a EPR study of $La_{2-x}Sr_xCuO_4$ (LSCO) with different oxygen isotopes (^{16}O and ^{18}O). This compound was doped with a few percent of Mn ions (1-2 %) which served as a EPR probe [46]. LSCO is particularly suitable for this kind of investigation. First of all, the structure of this compound is the simplest among the cuprates, containing a single Cu site which allows to dope Mn ions into the copper-oxygen layers. Furthermore, LSCO is the only cuprate superconductor for which the chemical composition can be varied over a wide enough range to obtain the full spectra of electronic properties: from an undoped antiferromagnetic to an overdoped metallic state. A symmetric EPR signal with a lineshape very close to Lorentzian and a g-value of 2.0 was observed in all samples. Fig. 12.9 shows the EPR signal of 2% Mn-doped $La_{1.94}Sr_{0.06}CuO_4$ for ^{16}O and ^{18}O isotope substituted samples. Note that the signal of the ^{16}O sample is stronger than that of the ^{18}O sample. The strong isotope effect observed in the EPR spectra is similar to our previous results obtained in the mixed valence perovskite manganite $La_{1-x}Ca_xMnO_{3+y}$ [47]. We have found that the isotope effect is strong in samples with small Sr doping (underdoped regime) and decreases with Sr concentration. An observation of the oxygen isotope effect on the EPR signal and its dependence on doping level in $La_{2-x}Sr_xCuO_4$ provides crucial information on the importance of the electron-phonon interaction in the spin dynamics of HTS and reflects the polaronic nature of the charge carriers in these compounds.

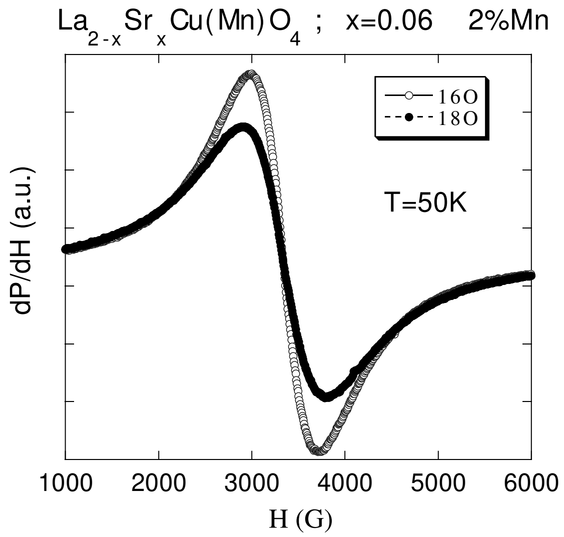

Figure 12.9: *EPR signal of* ^{16}O *and* ^{18}O *samples of* $La_{1.94}Sr_{0.06}Cu_{0.98}Mn_{0.02}O_4$ *measured at T=50 K under identical experimental conditions.*

References

[1] Y. Maeno *et al.*, Nature **372**, 532 (1994).

[2] A.P. Mackenzie *et al.*, Phys. Rev. Lett. **76**, 3786 (1996).

[3] T.M. Rice and M. Sigrist, J. Phys (Cond. Mat.) **7**, L643 (1995).

[4] D.F. Agterberg, T.M. Rice, M. Sigrist, Phys. Rev. Lett. **78**, 3374 (1997); D.F. Agterberg, preprint (cond-mat 9802151).

[5] T.M. Riseman *et al.*, Nature **396**, 242 (1998).

[6] C. M. Aegerter *et al.*, J. Phys. Cond. Mat **10**, 7445 (1998).

[7] D. McK. Paul *et al.*, Phys. Rev. Lett. **80**, 1517 (1998).

[8] G. Blatter, J. Rhyner, and V. M. Vinokur, Phys. Rev. B **43**, 7826 (1991).

[9] B. Keimer *et al.*, Phys. Rev. Lett. **73**, 3459 (1994); Science **262**, 83 (1993).

[10] S.T. Johnson *et al.* to be published in Phys. Rev. Lett. (1999); C. Ager *et al.* preprint.

[11] C.M. Aegerter *et al.*, Phys. Rev. B **57**, 1253 (1998); C.M. Aegerter *et al.* preprint.

[12] M. Roulin, A. Junod, and E. Walker, Science **273**, 1210 (1996); Physica C **296**, 137 (1998).

[13] A. Schilling *et al.*, Nature **382**, 791 (1996).

[14] M. Willemin *et al.*, Phys. Rev. Lett. **81**, 4236 (1998).

[15] A. Schilling *et al.*, Phys. Rev. Lett. **78**, 4833 (1997).

[16] See, e.g. H. Keller, in *Materials and Crystallographic Aspects of HTc-Superconductivity*, edited by E. Kaldis (Kluwer Academic Publishers, 1994), p.265; C.M. Aegerter and S.L. Lee, Applied Magnetic Resonance **13**, 75 (1997) and references therein.

[17] J.E. Sonier *et al.*, Phys. Rev. Lett. **72**, 744 (1994).

[18] A. Shengelaya *et al.*, Phys. Rev. B **58**, 3457 (1998).

[19] W.N. Hardy *et al.*, in *Proceedings of the 10th Anniversary HTS Workshop*, edited by B. Batlogg *et al.,* World Scientific, Singapore (1996).

[20] V.G. Kogan, Phys. Rev. B **24**, 1572 (1981); V.G. Kogan, M.M. Fang, and S. Mitra, Phys. Rev. B **38**, R11958 (1988).

[21] T. Schneider *et al.*, Eur. Phys. J. B **3**, 413 (1998); J. Hofer *et al.*, to appear in Phys. Rev. B.

[22] M. Willemin *et al.*, Phys. Rev. B **58**, R5940 (1998).

[23] C. Rossel *et al.*, Rev. Sci. Instrum. **69**, 3199 (1998).

[24] M. Willemin *et al.*, J. Appl. Phys. **83**, 1163 (1998).

[25] S. L. Lee *et al.*, Phys. Rev. Lett. **71**, 3862 (1993); U. Welp *et al.*, Phys. Rev. Lett. **76**, 4809 (1996); A. Schilling *et al.*, *Proceedings of the 10th Anniversary HTS Workshop on Physics, Materials and Applications, Houston, Texas, 1996*, edited by B.Batlogg *et al.*, (World Scientific, Singapore, 1996), p.349; A. Schilling *et al.*, Nature (London) **382**, 791 (1996).

[26] A. Schilling *et al.*, Phys. Rev. B **58**, 11157 (1998).

[27] M.J.W. Dodgson *et al.*, Phys. Rev. Lett. **80**, 837 (1998).

[28] A. Schilling and O. Jeandupeux, Phys. Rev. B **52**, 9714 (1995).

[29] G.M. Zhao *et al.*, Nature **381**, 676 (1996).

[30] K.-H, Höck, H. Nickisch, and H. Thomas, Helv. Phys. Acta. **56**, 237 (1983).

[31] M. Marezio *et al.*, Phys. Rev. Lett. **28**, 1390 (1972).

[32] C. H. Chen *et al.*, Phys. Rev. Lett. **71**, 2461 (1993).

[33] C. H. Chen *et al.*, Phys. Rev. Lett. **76**, 4042 (1996).

[34] M. Tokunaga *et al.*, Phys. Rev. B **57**, 5259 (1998).

[35] H. Kuwahara *et al.*, Science **270**, 961 (1995).

[36] Y. Tomioka *et al.*, Phys. Rev. Lett. **74**, 5108 (1995).

[37] V. I. Anisimov *et al.*, Phys. Rev. B **55**, 15494 (1997).

[38] S. K. Mishra *et al.*, Phys. Rev. B **56**, 2316 (1997).

[39] L. Sheng *et al.*, Phys. Rev. B **57**, 5265 (1997).

[40] J. M. Tranquada *et al.*, Nature (London) **375**, 561 (1995).

[41] H. A. Mook *et al.*, Nature (London) **395**, 580 (1998).

[42] A. Bianconi *et al.*, Phys. Rev. Lett. **76**, 3412 (1996).

[43] A. Lanzara *et al.*, Phys. Rev. B **55**, 9120 (1997).

[44] S. D. Conradson *et al.*, J. Supercond. **10**, 329 (1997).

[45] J.G. Bednorz and K.A. Müller, Z. Phys. B **64**, 189 (1986).

[46] B.I. Kochelaev *et al.*, Phys. Rev. B **49**, 13106 (1994).

[47] A. Shengelaya *et al.*, Phys. Rev. Lett. **77**, 5296 (1996).